Chinese Chemical Letters 36 (2025) 110408

Contents lists available at ScienceDirect

Chinese Chemical Letters

journal homepage: www.elsevier.com/locate/cclet

Azaindole-based asymmetric pentamethine cyanine dye for mitochondrial pH detection and near-infrared ratiometric fluorescence imaging of mitophagy

Tiancong Shi[a,1], Xi Chen[a,1], Xiao Zhou[a], Hongyi Zhang[a], Fuping Han[a], Lihan Cai[a], Wen Sun[a,b], Jianjun Du[a,b,*], Jiangli Fan[a,b,*], Xiaojun Peng[a]

[a] State Key Laboratory of Fine Chemicals, Frontier Science Center for Smart Materials, Dalian University of Technology, Dalian 116024, China
[b] Ningbo Institute of Dalian University of Technology, Ningbo 315016, China

ARTICLE INFO

Article history:
Received 8 July 2024
Revised 30 August 2024
Accepted 3 September 2024
Available online 3 September 2024

Keywords:
Asymmetric cyanine dye
pH probe
Mitochondria-targeting
Ratiometric fluorescence
Mitophagy

ABSTRACT

Mitochondria are crucial organelles responsible for maintaining cell growth, and their homeostasis is closely linked to pH regulation. Physiologically, mitochondria exhibit a weakly alkaline state (pH~8.0). However, when subjected to stress stimuli that cause damage, cells initiate the process of mitophagy, resulting in mitochondrial acidification. Therefore, monitoring changes in mitochondrial pH to comprehend the physiological processes associated with mitophagy is essential. In this study, we developed an asymmetric pentamethine cyanine dye **Cy5.5-H-CyN** as a probe for continuous monitoring of mitophagy in living cells. By incorporating an azaindole structure into the dye molecule, a ratiometric fluorescence response was achieved that is specifically responsive to pH variations while preserving its ability to target mitochondria and emit near-infrared fluorescence. Through various methods inducing mitophagy, **Cy5.5-H-CyN** was employed to determine mitochondrial pH quantitatively, demonstrating its suitability as an ideal probe for continuous monitoring of mitophagy in living cells.

Mitochondria generate energy through the respiratory chain to support numerous vital metabolic processes in cells [1,2]. Therefore, maintaining mitochondrial homeostasis is crucial for cellular growth [3]. Once damaged, mitochondria would be selectively sequestered with the following degradation process known as mitophagy [4]. Aberration in this process can contribute to various diseases, such as neurodegenerative and cardiovascular disorders [5]. Interestingly, the occurrence of mitophagy usually results in a significant reduction in mitochondrial pH, from approximately pH 8.0 under normal physiological conditions to around pH 5.5–6.5 [6]. Therefore, developing a real-time and accurate method for detecting mitochondrial pH values holds immense significance in comprehending the pivotal functions of mitochondria under both physiological and pathological circumstances.

Small molecule fluorescent probes possess the advantages of non-invasiveness, high sensitivity, and good specificity, which are extensively utilized in imaging physiological processes within living cells [7-10]. Currently, reported mitophagy probes primarily utilize naphthalimide or rhodamine derivatives. For example, Kim *et al.* developed the naphthalimide-based probe to monitor mitophagy, incorporating piperazine as a proton binding site and triphenylphosphine as the mitochondrial targeting group [11]. Zhang *et al.* designed a rhodamine-derived ratiometric pH fluorescent probe targeted explicitly to mitochondria for visualizing pH alterations during rapamycin-induced mitophagy [12]. To summarize, the probes employed for monitoring the mitophagy process must fulfill three fundamental requirements: (i) Excellent mitochondrial targeting capability, (ii) sensitive pH responsiveness, and (iii) emission wavelength located in the "near-infrared (NIR) window" (650–900 nm) of biological imaging [13]. Therefore, neither naphthalimide nor rhodamine derivatives are ideal mitophagy probes because most of their emission wavelengths are centered at 350–600 nm. Cyanine dyes usually exhibit instinctive capability in targeting mitochondria because of their cationic structure [14,15], and the multi-methine structure's derivatization allows emission wavelength adjustment to the "NIR window" [16]. Nevertheless, normal cyanine dyes lack pH-responsive functional group [17,18]. Azaindole was developed and introduced in our former works to construct the NIR photosensitizers [19]. Besides enlarging the conjugation system, the exposed indole nitrogen in azaindole is also an excellent proton-binding site for pH response [20,21].

* Corresponding authors.
E-mail addresses: dujj@dlut.edu.cn (J. Du), fanjl@dlut.edu.cn (J. Fan).
[1] These authors contributed equally to this work.

https://doi.org/10.1016/j.cclet.2024.110408
1001-8417/

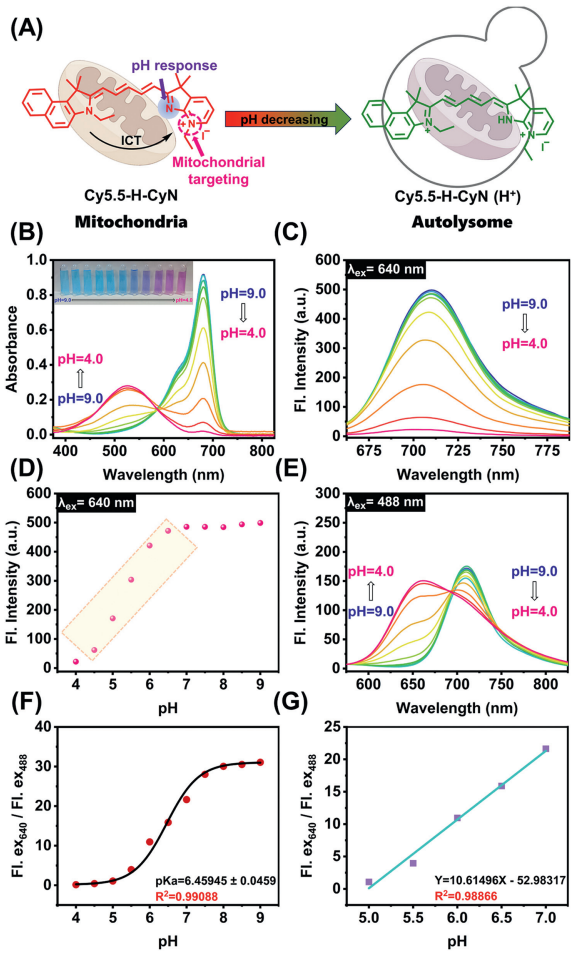

Fig. 1. (A) The chemical structure and pH sensing mechanism of **Cy5.5-H-CyN** in mitochondria. (B) The pH-dependent absorbance spectra of **Cy5.5-H-CyN** (Inset: the solution color of **Cy5.5-H-CyN** in PBS with different pH values). (C) The pH-dependent emission spectra of **Cy5.5-H-CyN** ($\lambda_{ex} = 640$ nm). (D) The fluorescence intensity of **Cy5.5-H-CyN** in PBS at different pH values ($\lambda_{ex} = 640$ nm). (E) The pH-dependent emission spectra of **Cy5.5-H-CyN** ($\lambda_{ex} = 488$ nm). (F) The fluorescence intensity ratio Fl. $\lambda_{ex\ 640\ nm}$/Fl. $\lambda_{ex\ 488\ nm}$ *vs.* pH (4.0–9.0). (G) Linear fitting of Fl. $\lambda_{ex\ 640\ nm}$/Fl. $\lambda_{ex\ 488\ nm}$ *vs.* pH (5.0–7.0).

As a proof of concept, an asymmetric pentamethine cyanine dye, **Cy5.5-H-CyN**, was constructed to continuously monitor the mitophagy process in living cells (Fig. 1A). Incorporating azaindole preserved not only the intrinsic mitochondrial targeting ability but also redshifted fluorescence emission to the "NIR window". Moreover, upon proton binding, the intramolecular charge transfer (ICT) effect of **Cy5.5-H-CyN** was attenuated, enabling the generation of ratiometric fluorescence signals for pH at two emission wavelengths (662 and 710 nm). Notably, **Cy5.5-H-CyN** exhibits a robust linear relationship within the pH range of 5.0–7.0 in both solution and cellular environments. The response of **Cy5.5-H-CyN** to pH variations is rapid, sensitive, and reversible. Importantly, by utilizing ratio fluorescence signals, quantitative analysis of mitochondrial pH can be achieved under diverse mitophagy stimulation conditions, such as rapamycin, thus facilitating real-time monitoring of the mitophagy process.

Cy5.5-H-CyN was synthesized *via* a four-step route, and **Cy5.5-H-Cy5** was prepared as a reference compound. The synthesis process was described in detail in Scheme S1 (Supporting information). Both compounds were characterized by ^{1}H nuclear magnetic resonance spectroscopy (NMR), ^{13}C NMR, and high-resolution mass spectroscopy (HRMS). The characterizations are shown in Figs. S1–S8 (Supporting Information). Additionally, single-crystal X-ray diffraction analysis was employed to confirm the structure of **Cy5.5-H-CyN**, as shown in Fig. S9A (Supporting information). The **Cy5.5-H-CyN** exhibited an interlaced arrangement with parallel orientation in the crystal lattice (Fig. S9B and Table S1 in Supporting information).

Firstly, the spectral behavior of molecules with varying pH was investigated. The absorbance of **Cy5.5-H-CyN** at 678 nm gradually decreased as the pH changed from 9.0 to 4.0, while the absorbance at 526 nm increased simultaneously, with a blue-to-pink color change of the solution (Fig. 1B). Uniform parameter settings were employed for testing to ensure consistency for subsequent intracellular fluorescence imaging. When the probe was excited at 640 nm, there was no significant change in fluorescence at 710 nm (Fl. $\lambda_{ex\ 640\ nm}$) within a pH range of 7.0–9.0 (Fig. 1C). However, below pH 7.0, Fl. $\lambda_{ex\ 640\ nm}$ exhibited a noticeable decrease (Fig. 1D). This phenomenon can be attributed to the weakening of the ICT process following the protonation of the indole nitrogen atom in **Cy5.5-H-CyN**, resulting in a blue shift in molecular absorption wavelength and pronounced fluorescence quenching. These findings fully demonstrate that **Cy5.5-H-CyN** possesses pH-responsive capabilities and exhibits fluorescent changes within the mitophagy-relevant pH range. However, due to the absence of proton-binding sites, **Cy5.5-H-Cy5** did not possess pH-responsive capability, resulting in no absorption and fluorescence changes with pH changes (Fig. S10 in Supporting information). When the probe was excited at 488 nm, a gradually intensified fluorescence peak (Fl. $\lambda_{ex\ 488\ nm}$) was observed at 662 nm (Fig. 1E) as buffer pH decreased, corresponding to the absorption peak at 526 nm and representing the fluorescence peak of the **Cy5.5-H-CyN** structure after proton binding occurred, the specific absorbance values corresponding to the two wavelengths are presented in Table S2 (Supporting information). Both fluorescence emissions are located within the "NIR window", which enhances cell imaging by reducing background interference [22]. The pH and the corresponding Fl. $\lambda_{ex\ 640\ nm}$/Fl. $\lambda_{ex\ 488\ nm}$ value can be fitted to an "S" curve based on the Henderson-Hasselbalch equation. The pK_a value of **Cy5.5-H-CyN** was approximately 6.5 ($R^2 = 0.99$) (Fig. 1F). Moreover, there was a robust linear relationship between Fl. $\lambda_{ex\ 640\ nm}$/Fl. $\lambda_{ex\ 488\ nm}$ and pH values ranging from 5.0 to 7.0 ($R^2 = 0.99$) (Fig. 1G). These results demonstrated that **Cy5.5-H-CyN** exhibited excellent ratiometric fluorescence response for accurately monitoring pH changes.

Water solubility is a critical parameter for bioimaging probes [23]. To demonstrate the solubility of **Cy5.5-H-CyN** under both mitochondrial physiological and acidic conditions, absorption spectra were measured at 678 nm (pH 8.0) and 526 nm (pH 4.0) for probes with increasing concentrations, and then the absorbance values were then correlated with the respective concentrations through fitting analysis. Remarkably, there was an excellent linear relationship between absorbance intensities and probe concentrations under both pH conditions (Fig. S11 in Supporting information). The comprehensive description of the additional photophysical properties of **Cy5.5-H-CyN** were provided in Tables S3 and S4 (Supporting information).

To further investigate the adaptability of **Cy5.5-H-CyN** in monitoring mitophagy in living cells, pH cycle testing was conducted. As shown in Fig. S12 (Supporting information), after 4 cycles, **Cy5.5-H-CyN** still demonstrated satisfactory reversibility of fluorescence intensity with little loss (Fig. S12A), indicating its excellent response to pH changes for real-time pH monitoring. Subsequently, the selectivity of **Cy5.5-H-CyN** towards common biological disruptors, including metal cations, anions, reactive oxygen species, biothiols, and amino acids, was evaluated. At pH 7.4, the above chemicals did not interfere with the fluorescence properties of **Cy5.5-H-CyN** (Fig. S12B), highlighting its specific response to pH in complex biological environments, such as living cells and organelles. The flu-

orescence intensity of **Cy5.5-H-CyN** was recorded every minute for 30 min under both pH conditions, and there was no significant change (Fig. S12C), confirming its fluorescence stability. To investigate the impact of viscosity on the testing process, mixed solutions containing ethanol and 1,5-pentanediol were prepared with different proportions. The fluorescence spectra of **Cy5.5-H-CyN** and **Cy5.5-H-Cy5** in solutions with different viscosities were measured, and I/I_0 (the ratio of fluorescence intensity (I) to initial fluorescence intensity (I_0)) was calculated to assess the effect. As shown in Fig. S12D, the I/I_0 increase for **Cy5.5-H-CyN** was smaller than that of **Cy5.5-H-Cy5**, indicating that **Cy5.5-H-CyN** is insensitive to viscosity. These results demonstrated that **Cy5.5-H-CyN** exhibits high stability and selectivity for pH determination.

DFT calculations were performed to further investigate the mechanism underlying the alteration of photophysical properties utilizing the M062X/def2svp functional and basis set in **Cy5.5-H-CyN** upon proton binding (Fig. S13A in Supporting information). Solvation effects were considered using a water medium in the SMD model. All calculations were performed using Gaussian 16 A software, with electron-hole analysis conducted using Multiwfn 3.8 [24,25]. The frontier molecular orbitals (FMO) energy of the ground state (S_0) and singlet excited state (S_1) are depicted in Fig. S13B (Supporting information). From an energetic perspective, the protonation of **Cy5.5-H-CyN (H^+)** resulted in a more stable the highest occupied molecular orbital (HOMO) arrangement than its deprotonated form, leading to an apparent energy reduction ($-6.73 \rightarrow -5.98$ eV). However, minimal changes were observed in the lowest unoccupied molecular orbital (LUMO) energy ($-2.21 \rightarrow -2.00$ eV). Consequently, this substantial increase in the HOMO-LUMO energy gap of **Cy5.5-H-CyN (H^+)** ($-3.98 \rightarrow -4.52$ eV) required more energy for electron transition and caused a blue shift in the absorption wavelength (Fig. 1B). The combination of protons results in a slight increase in HOMO-LUMO of the energy gap for the S_1 state, leading to a blue shift of emission wavelength consistent with experimental observations (Table S2). Therefore, the protonation induced significant alterations in the FMO, potentially influencing electronic distribution in excited states.

The electron-hole distribution before and after proton binding was analyzed to explore electron transfer characteristics in the excited state (Fig. S14 in Supporting information). The atomic contribution heat map revealed that in S_0 coordinates, both sides of deprotonated **Cy5.5-H-CyN** exhibited significant contributions from indole groups to holes (58.7%) and electrons (56.5%). However, upon proton binding, this contribution decreased to 32.7% for holes and 49.6% for electrons with more concentration on the methine chain, resulting in a notable decrease in ICT as well as a more significant blue shift in wavelength. In the S_1 coordinate, regardless of proton binding, both sides of the indole groups demonstrated electron-donating properties, with hole contributions exceeding electron contributions. After proton binding occurred due to the weakened electron-donating ability of azaindole moiety, hole contribution moderately reduced (59.4% → 54.8%), weakening the ICT effect, leading to a blue shift in emission wavelength.

Before the experiment in living cells, the toxicity of **Cy5.5-H-CyN** to HeLa cells was assessed using the MTT assay. Upon reaching a concentration of 8 μmol/L, the cytotoxicity of **Cy5.5-H-CyN** decreased to below 80% (Fig. S15 in Supporting information), indicating its favorable biocompatibility at low doses. To investigate the mitochondrial targeting ability, **Cy5.5-H-CyN** was co-stained with MitoTracker Green FM (a commercial dye for mitochondria) in HeLa cells. The fluorescence distribution of **Cy5.5-H-CyN** exhibited excellent overlap with that of MitoTracker Green FM (Pearson coefficient: 0.871) (Fig. S16 in Supporting information). Conversely, there was little overlap observed between **Cy5.5-H-CyN** and LysoTracker Green DND 26 (a lysosomal targeting dye) as well as Hoechst 33342 (a nuclear targeting dye) with Pearson coefficient of 0.486 and 0.076, respectively (Fig. S17 in Supporting information). This marked disparity highlights the exceptional mitochondrial specificity of **Cy5.5-H-CyN**.

The decrease in mitochondrial membrane potential (MMP) is a key characteristic of mitophagy [4]. However, the reduction or disappearance of MMP can result in the leakage of normal probes, which target mitochondria based on electrostatic attraction, thereby compromising the accuracy of the test [26]. To assess the targeting ability of **Cy5.5-H-CyN**, a mitochondrial uncoupling experiment was conducted. CCCP, a commonly used uncoupling reagent for mitochondrial proton carriers, rapidly dissipates the H^+ gradient across the inner membrane within 5 min, leading to acidification of mitochondria and reduction in MMP [27]. Specifically, **Cy5.5-H-CyN** was incubated with HeLa cells for 1 h, washed with DMEM medium three times, and subsequently co-incubated with CCCP and MitoTracker Green FM for 30 min. Rhodamine 123 (a fluorescent dye possessing mitochondrial targeting ability) was employed as a control. Surprisingly, upon the addition of CCCP, the fluorescence intensity of **Cy5.5-H-CyN**-treated cells only exhibited a slight decrease, and the distribution pattern of fluorescence remained comparable to that observed with MitoTracker Green FM. Notably, it continued to exhibit enrichment within mitochondria (Pearson coefficient: 0.908–0.892) (Fig. S18 in Supporting information). However, the fluorescence intensity of rhodamine 123 in the control group essentially vanished (Fig. S19 in Supporting information). Therefore, **Cy5.5-H-CyN** can effectively localize within mitochondria without the influence of changes in MMP. We proposed that **Cy5.5-H-CyN**, similar to mitochondrial respiratory inhibitors, could bind a specific protein within the mitochondrial respiratory chain [28], enhancing its affinity with mitochondria. To validate this hypothesis, we evaluated the ATP levels in HeLa cells after the addition of **Cy5.5-H-CyN**. As illustrated in Fig. S20 (Supporting information), introducing **Cy5.5-H-CyN** resulted in a noticeable reduction in ATP levels within HeLa cells compared to the control group. For example, with the introduction of 6 μmol/L **Cy5.5-H-CyN**, the ATP levels were approximately 70% lower than in the control group. These findings proved that **Cy5.5-H-CyN** indeed enhanced its ability to localize mitochondria by binding to proteins within the respiratory chain.

To quantitatively determine the pH value in mitochondria, it is necessary to calibrate the intracellular pH. HeLa cells were initially incubated with **Cy5.5-H-CyN** and then replaced with PBS containing nigericin (10 μmol/L) at various pH levels for a specific incubation period before cell imaging was conducted. As expected, when the pH decreased from 8.0 to 4.0, fluorescence decreased in the red channel while it increased in the green channel. The ratio in the merged channel transitioned gradually from red (pH 8.0) to orange and eventually turned green (pH 4.0). Additionally, the ratio of fluorescence signal between the red and green channels also changed progressively from red-green at pH 8.0 to blue-green until it essentially disappeared at pH 4.0 (Fig. 2A). Subsequently, the quantitative relationship between the fluorescence intensity ratio Fl. $\lambda_{ex\ 640\ nm}$/Fl. $\lambda_{ex\ 488\ nm}$ and pH were analyzed (Fig. 2B). In HeLa cells, **Cy5.5-H-CyN** exhibited a linear response range (pH 5.0–7.0), consistent with the results obtained in solution (Fig. 2C). These findings indicate that **Cy5.5-H-CyN** can precisely track and visualize mitochondrial pH changes in live cells. When mitochondria were damaged by stress stimulation, to maintain cellular homeostasis and mitochondrial function, damaged mitochondria would undergo mitophagy and fuse with lysosomes to form autolysosomes, resulting in a pH decrease in mitochondria.

To investigate the ability of **Cy5.5-H-CyN** to monitor the process of mitophagy in living cells, various methods were employed to induce mitophagy. As mentioned earlier, mitochondrial uncouplers can reduce MMP, trigger mitophagy, and acidify mitochondria. However, at lower doses, mitochondrial uncouplers rapidly re-

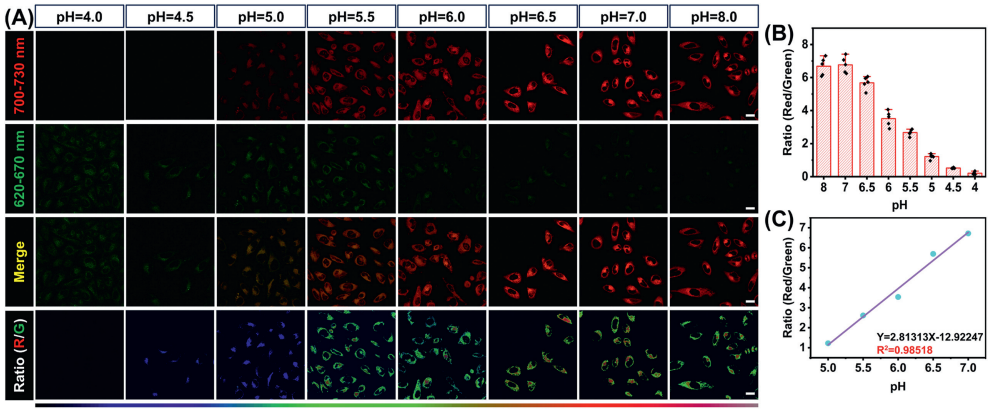

Fig. 2. Calibration of intracellular pH in HeLa cells with **Cy5.5-H-CyN**. (A) Fluorescence imaging of HeLa cells after incubation with **Cy5.5-H-CyN** and different pH buffers containing 10 μmol/L nigericin. Red channel: $\lambda_{ex} = 640$ nm, $\lambda_{em} = 700–730$ nm; Green channel: $\lambda_{ex} = 488$ nm, $\lambda_{em} = 620–670$ nm. Ratio channel: red channel/green channel. Scale bar: 20 μm. (B) Ratio channel fluorescence intensity diagram of different pH in HeLa cells. The data are expressed as the mean ± SD of five measurements. (C) The linear relationship between the ratio channel fluorescence intensity and pH in HeLa cells.

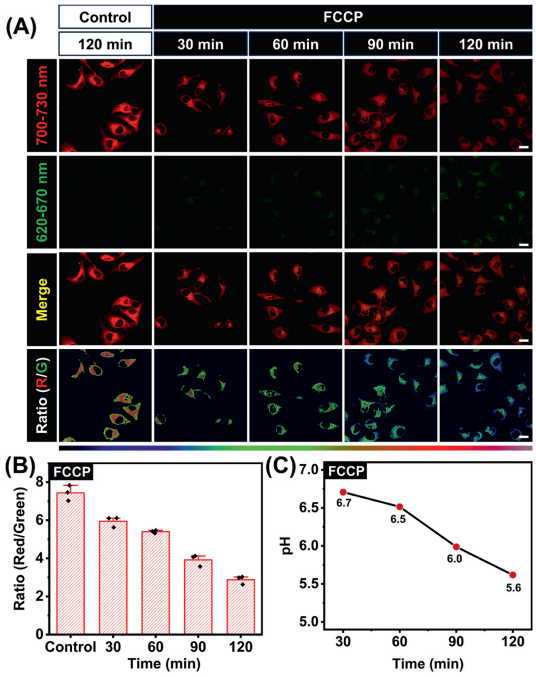

Fig. 3. (A) Fluorescence imaging of **Cy5.5-H-CyN** in HeLa cells at different times after incubation with FCCP. Red channel: $\lambda_{ex} = 640$ nm, $\lambda_{em} = 700–730$ nm; Green channel: $\lambda_{ex} = 488$ nm, $\lambda_{em} = 620–670$ nm. Ratio channel: red channel/green channel. Scale bar: 20 μm. (B) The fluorescence intensity of **Cy5.5-H-CyN** ratio channel in HeLa cells at different times after incubation with FCCP. The data were expressed as mean ± SD of three measurements. (C) The mitochondrial pH of HeLa cells at different times after incubation with FCCP.

duce MMP and exhibit poor ability to acidify mitochondria (for example, 10 μmol/L CCCP only reduced the pH of mitochondria from 7.8 to 7.2 [29]). Therefore, for visualization of the process of mitophagy by **Cy5.5-H-CyN** without effects on cell viability, HeLa cells were treated with a concentration of 50 μmol/L FCCP to trigger mitophagy. The fluorescence imaging results demonstrated a significant decrease in the fluorescence intensity in the red channel after incubation with FCCP for only 30 min, compared to the control group. Furthermore, for 120 min, the fluorescence intensity of the red channel was remarkably lowered, while the green channel exhibited obvious fluorescence signals (Figs. 3A and B). By utilizing the fluorescence ratio between two channels and referring to a pH calibration curve, it is possible to calculate that mitochondrial pH decreased from approximately 6.7 (at 30 min) to around 5.6 (at 120 min) (Fig. 3C).

Rapamycin, a widely utilized anticancer medication, could inhibit cell proliferation through the suppression of the mammalian targets of the rapamycin signaling pathway, which can induce mitophagy in various cells [26]. Following incubation with **Cy5.5-H-CyN** in HeLa cells, rapamycin (5 μmol/L) was introduced to stimulate mitophagy. The imaging results demonstrated that compared to the control group, there was a significant reduction in fluorescence intensity in the red channel after 6 h and obvious fluorescence signals were observed in the green channel after 12 h (Figs. 4A and B). Based on the pH calibration curve, it can be calculated that rapamycin-induced mitophagy in HeLa cells with a mitochondrial pH change from approximately 6.0 at 6 h to around 5.6 after 12 h (Fig. 4C).

The deficiency of cell nutrients or growth under hypoxic conditions can inhibit cellular metabolism and disrupt mitochondrial function, thereby triggering mitophagy [6,30]. Therefore, HeLa cells were incubated with **Cy5.5-H-CyN** and imaged using serum-free medium or hypoxic condition (1% O_2). The imaging results revealed a significant reduction in fluorescence intensity in the red channel after 6 h under both culture conditions, and the green channel exhibited noticeable fluorescence signals after 12 h (Fig. 4A). Based on the pH calibration curve, it was determined that nutrient deficiency or hypoxia resulted in mitochondrial pH levels of approximately 6.4 and 6.2 after 6 h and reached around 6.0 and 5.7 after 12 h, respectively (Figs. 4D and E). All these experimental findings demonstrated that the application of **Cy5.5-H-CyN** enabled quantitative visualization of mitochondrial pH to monitor the process of mitophagy.

In the advanced stage of mitophagy, lysosomes fuse with mitophagosomes to degrade mitochondria, thereby maintaining intracellular homeostasis [4]. During this phase, the fusion of these organelles induces alterations in the corresponding co-localization coefficients as observed through cellular fluorescence imaging. To elucidate this process, **Cy5.5-H-CyN** was employed as a probe for monitoring mitophagy and commercially available dyes of MitoTracker Green FM and LysoTracker Red DND 99 were utilized as indicators for mitochondria and lysosomes respectively. By employing various established conditions to induce mitophagy, changes in the co-localization coefficients were observed among these three components. As shown in Figs. S21A and B (Supporting information), where **Cy5.5-H-CyN**, MitoTracker Green FM, and LysoTracker Red DND 99 were assigned to the blue, green, and red channels respectively for visualization purposes. The control group was maintained under normal culture conditions. Following incubation with

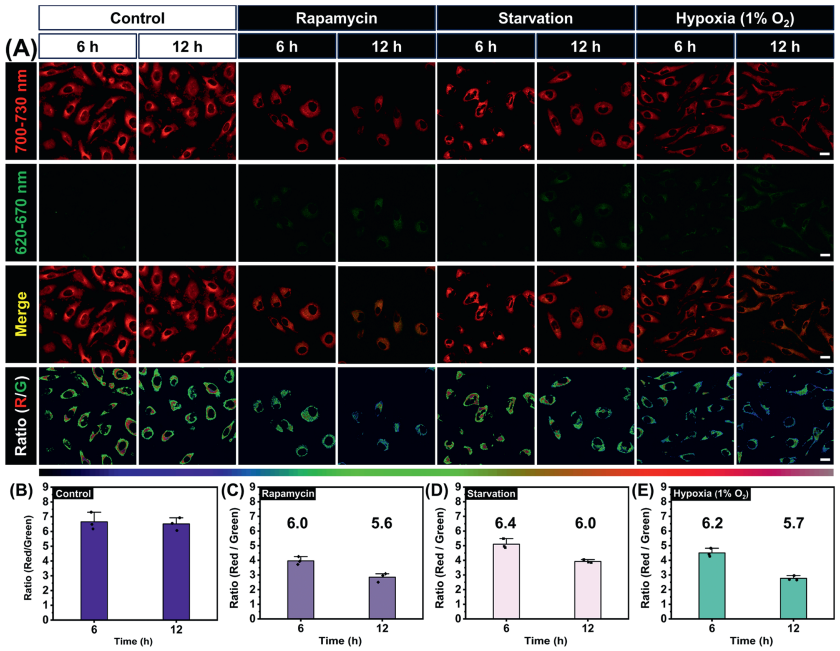

Fig. 4. (A) Fluorescence imaging of HeLa cells after incubation with **Cy5.5-H-CyN** and treatment with different mitophagy induction methods. Red channel: $\lambda_{ex} = 640$ nm; $\lambda_{em} = 700–730$ nm; Green channel: $\lambda_{ex} = 488$ nm, $\lambda_{em} = 620–670$ nm; Ratio channel: Red channel/Green channel. Scale bar: 20 μm. (B–E) The ratio fluorescence intensity of **Cy5.5-H-CyN** in HeLa cells was treated with different mitophagy induction methods at different times. The value is the corresponding pH value. The data are expressed as the mean ± SD of three measurements.

Cy5.5-H-CyN, MitoTracker Green FM and LysoTracker Red DND 99 were subsequently added into cells. Co-localization coefficients in the blue-green and blue-red channels indicated mitochondrial localization of **Cy5.5-H-CyN**. Under normal conditions, a low colocalization coefficient in the green-red channel suggested distinct separation and minimal fusion between mitochondria and lysosomes. However, upon application of various mitophagy induction methods for a specific duration, there was an obvious increase in the green-red co-localization coefficient, indicating fusion events between these organelles during mitophagy process. Moreover, a significant decrease in the blue-green co-localization coefficient along with a marked increase in the blue-red co-localization coefficient further supported this phenomenon. Therefore, utilizing **Cy5.5-H-CyN** as a probe for long-term dynamic monitoring of mitophagy is highly feasible.

In summary, an azaindole-based asymmetric pentamethine cyanine dye **Cy5.5-H-CyN** was designed and easily synthesized, exhibiting NIR fluorescence, excellent mitochondrial targeting, and sensitive and reversible pH response-ability. Linear relationships were obtained within the pH range of 5.0–7.0 in both aqueous solution and intracellular media. By employing various mitophagy induction methods, real-time and quantitative ratiometric fluorescence imaging of mitochondrial pH changes was successfully achieved during mitophagy in HeLa cells. Therefore, **Cy5.5-H-CyN** not only provides a promising tool for monitoring pH changes during mitophagy but also offers an effective means to investigate the role of mitophagy in diverse intracellular pathological processes. This asymmetric multi-methine structure enables further extension of the emission wavelength by elongating the methine chain, thereby enhancing imaging depth and minimizing autofluorescence interference.

Declaration of competing interest

The authors declare that they have no known competing financial interests or personal relationships that could have appeared to influence the work reported in this paper.

CRediT authorship contribution statement

Tiancong Shi: Writing – original draft, Validation, Methodology, Data curation, Conceptualization. **Xi Chen:** Software, Formal analysis. **Xiao Zhou:** Software. **Hongyi Zhang:** Resources. **Fuping Han:** Methodology. **Lihan Cai:** Resources. **Wen Sun:** Methodology, Formal analysis. **Jianjun Du:** Writing – review & editing, Visualization, Supervision, Conceptualization. **Jiangli Fan:** Supervision, Project administration, Funding acquisition. **Xiaojun Peng:** Supervision, Project administration, Funding acquisition.

Acknowledgments

This work was financially supported by the Fundamental Research Funds for the Central Universities (Nos. DUT23YG137 and DUT22LAB601), Liaoning Binhai Laboratory (No. LBLB-2023-03), Liaoning Province Science and Technology Joint Fund (Nos. 2023JH2/101800039 and 2023JH2/101800037), National Natural Science Foundation of China (Nos. 21925802, 22090011, and 21878039).

Supplementary materials

Supplementary material associated with this article can be found, in the online version, at doi:10.1016/j.cclet.2024.110408.

References

[1] J. Nunnari, A. Suomalainen, Cell 148 (2012) 1145–1159.
[2] A. Picca, J. Faitg, J. Auwerx, L. Ferrucci, D. D'Amico, Nat. Metab. 5 (2023) 2047–2061.
[3] H.M. Ni, J.A. Williams, W.X. Ding, Redox Biol. 4 (2015) 6–13.
[4] R.J. Youle, D.P. Narendra, Nat. Rev. Mol. Cell Biol. 12 (2011) 9–14.
[5] L. Wang, B. Chen, P. Peng, et al., Chin. Chem. Lett. 28 (2017) 1965–1968.
[6] R. Yadav, S. Munan, M. Ali, K. Mapa, A. Samanta, Chem. Asian J. 18 (2023) e202300308.
[7] P. Ning, W. Wang, M. Chen, et al., Chin. Chem. Lett. 28 (2017) 1943–1951.
[8] S. Munan, M. Ali, R. Yadav, K. Mapa, A. Samanta, Anal. Chem. 94 (2022) 11633–11642.
[9] Y. Zhang, Y. Chen, H. Fang, et al., J. Mater. Chem. B 10 (2022) 5422–5429.

[10] Y. Zhang, Z. Li, W. Hu, Z. Liu, Anal. Chem. 91 (2019) 10302–10309.
[11] M.H. Lee, N. Park, C. Yi, et al., J. Am. Chem. Soc. 136 (2014) 14136–14142.
[12] W. Shu, J. Yu, Z. Li, et al., Sens. Actuator. B: Chem. 369 (2022) 132323.
[13] C. Yan, L. Shi, Z. Guo, et al., Chin. Chem. Lett. 30 (2019) 1849–1855.
[14] F. Han, S.A. Abbas Abedi, S. He, et al., Adv. Sci. 11 (2024) 2305761.
[15] H. Ma, Y. Lu, Z. Huang, et al., J. Am. Chem. Soc. 144 (2022) 3477–3486.
[16] W. Sun, S. Guo, C. Hu, J. Fan, X. Peng, Chem. Rev. 116 (2016) 7768–7817.
[17] Y. Ma, Y. Liu, Z. Jiang, et al., Sens. Actuator. B: Chem. 349 (2021) 130747.
[18] Y. Liu, J. Zhou, L. Wang, et al., J. Am. Chem. Soc. 138 (2016) 12368–12374.
[19] H. Huang, D. Huang, M. Li, et al., Dyes Pigm. 177 (2020) 108284.
[20] Y. Wang, Z. Lei, C. Wang, et al., RSC Adv. 11 (2021) 17871–17879.
[21] J.R. Hou, D. Jin, B. Chen, et al., Chin. Chem. Lett. 28 (2017) 1681–1687.
[22] R. Wang, Y. Xing, R. Wang, et al., Coord. Chem. Rev. 513 (2024) 215866.
[23] J. Huang, J. Huang, P. Cheng, Y. Jiang, K. Pu, Adv. Funct. Mater. 30 (2020) 2003628.
[24] T. Lu, F. Chen, J. Comput. Chem. 33 (2012) 580–592.
[25] Z. Liu, T. Lu, Q. Chen, Carbon 165 (2020) 468–475.
[26] X. Li, Y. Hu, X. Li, H. Ma, Anal. Chem. 91 (2019) 11409–11416.
[27] X. Luo, W. Xiang, Y. Lu, et al., Chem. Eng. J. 488 (2024) 151169.
[28] Q. Wang, T. Yang, S. Li, et al., Research 6 (2023) 0223.
[29] Y. Chen, C. Zhu, J. Cen, et al., Chem. Sci. 6 (2015) 3187–3194.
[30] S.K. Dwivedi, D.L. Arachchige, T. Vohs, et al., J. Mater. Chem. B 11 (2023) 2852–2861.